Date of publication xxxx 00, 0000, date of current version xxxx 00, 0000.

Digital Object Identifier –.—/ACCESS.2020.DOI

Decoupled Downlink and Uplink Access for Aerial Terrestrial Heterogeneous Cellular Networks

MOHAMMAD ARIF[1], SHURJEEL WYNE[1], (SENIOR MEMBER, IEEE), KEIVAN NAVAIE[2], (SENIOR MEMBER, IEEE), SYED JUNAID NAWAZ[1], (SENIOR MEMBER, IEEE), AND SAJID HUSSAIN ALVI[3] .

[1]Department of Electrical and Computer Engineering, COMSATS University Islamabad (CUI), Islamabad-45550, Pakistan (e-mail: shurjeel.wyne@comsats.edu.pk and e-mail: junaidnawaz@ieee.org)
[2]School of Computing and Communications, Lancaster University, Lancaster LA1 4WA, U.K. (e-mail: k.navaie@lancaster.ac.uk)
[3]Department of Physics, COMSATS University Islamabad (CUI), Islamabad-45550, Pakistan (e-mail: sajid_hussain@comsats.edu.pk)

Corresponding author: Mohammad Arif (e-mail: mohammadarif911@gmail.com).

This work was supported in part by the EU-funded project ATOM-690750 under call H2020-MSCA-RISE-2015 and in part by the UK Engineering and Physical Sciences Research Council (EPSRC) under Grant EP/S009620/1.

ABSTRACT To enable reliable connectivity in highly dynamic and dense communication environments, aerial-terrestrial heterogeneous cellular networks (AT-HCNs) have been proposed as a plausible enhancement to the conventional terrestrial HCNs (T-HCNs). In busy urban scenarios, users are often located in clusters and demand high bandwidth in both downlink (DL) and uplink (UL). We investigate this scenario and model the spatial distribution of clustered users using a Matern cluster process (MCP). Based on our analysis we then argue that decoupling of DL and UL in such a setting can significantly improve coverage performance and spectral efficiency. We further obtain closed-form expressions for the system coverage probability, spectral efficiency, and energy efficiency by using the Fox H-function. The main results confirm the validity of the proposed analytical modeling. Our simulations further indicate a significant performance improvement using decoupled access and provide quantitative insights on AT-HCN system design.

INDEX TERMS Heterogeneous cellular networks, Downlink and uplink decoupling, Matern cluster process, Poisson point process, Unmanned aerial vehicles.

I. INTRODUCTION

The innovative technologies and services offered by 5th generation (5G) wireless networks, along with promising performance improvements, are expected to bring a tremendous proliferation in the scale of wireless networks, mobile data demands, and network services types. The global machine-type and mobile-user subscribers are estimated to reach 97bn and 17.1bn, respectively, by the year 2030 [1]. This anticipated ultra-massive increase in the scale and dimensions of wireless networks in the beyond 5G (B5G) era is admitted to lead to the scarcity of network capacity and degradation in the quality of service (QoS) [2]. Evolution in the size of cells from small to tiny and the nature of base stations (BSs) from terrestrial-fixed to aerial-vehicular are among the promising research directions to design spectrum-, energy-, and cost-efficient wireless networks. Such aerial and terrestrial BSs integrated volumetric heterogeneous networks hold the capability to more aggressively and smartly reuse the network resources, create favorable channel conditions for the users in ultra-dense urban environments, extend network coverage to remote and/or vehicular nodes, meet the occasional ultra-high data demands during exclusive events (e.g., concerts, sports, etc.), and assist in different emergency and monitoring services (e.g., disasters, accidents, etc.), to name a few.

A. MOTIVATION AND RELATED WORK

One of the promising solutions to achieve a better QoS in an ultra-dense urban environment is to implement low-power small base stations (SBSs) in tandem with the high-power macro BS (MBS) in the terrestrial heterogeneous cellular network (T-HCNs) [3]. As an alternative to (or enhancement of) the T-HCN for the cases, such as emergencies, exclusive events, and ultra-dense urban environments, deployment of unmanned aerial vehicles (UAVs) is also considered as highly

significant in resolving the network economic constraints [4]–[6]. UAVs-based BSs also help in ensuring favorable channel conditions (through provisioning line-of-sight (LoS) link) for the user equipments (UEs), which leads to significant improvement in the performance of such aerial heterogeneous cellular networks (A-HCNs). In this regard, an increase in the number of serving UAVs can further improve the network performance by offloading a notable amount of traffic from the terrestrial access network [7], [8]. To ensure appropriate deployment of such UAVs encompasses several critical considerations based on their size, weight, and power-availability [9]. The UAVs with battery constraints, low transmission power, less payload capacity, less weight, and limited mobility capability are usually deployed as low altitude platforms (LAPs); whereas, high altitude platforms (HAPs) possess extended coverage, higher altitude, and extensive endurance capabilities.

The performance of A-HCNs is affected by the spatial distribution of the ground users. The authors in [10]–[13] model UEs according to an independent homogeneous Poisson point process (HPPP) and investigate the impact of altitude and density on the coverage performance. Similarly, [14], [15] analyzes the outage performance of the network and shows that the outage probability increases with an increase in the number of UAVs. However, HPPP based modeling cannot accurately reflect the nature of interference in clustered scenarios [16]–[20]. For instance, in an earthquake or flood-affected areas (such as at refuge camps or local tents), where the traditional infrastructure is destroyed and the UEs are present in clusters. In such scenarios, clustering should be accurately modeled to predict the network's performance.

A-HCN is a viable alternative for providing coverage to the clustered users. For such clustered users, the work in [21]–[24] analyzes coverage and area spectral efficiency (SE) by modeling the UEs as a Matern cluster process (MCP). Therein, authors show that accurate characterization of clustering behavior (if it is present in the considered environment) plays a vital role in both the design and performance of the network. MCP constitutes of parent nodes and child nodes, where the parent nodes are considered as uniformly distributed according to an independent HPPP. For each parent node, the distribution of associated child nodes is modeled by an independent and identical spatial distribution confined within a circularly shaped region with parent node at its origin. The parent nodes themselves are not part of the clustering process [25], [26].

In addition to the spatial distribution of the users, user-association also plays a vital role in determining system performance. Conventionally in T-HCNs, it is assumed that for each UE, BS association is based on a DL-reference received power, where both DL and UL are provisioned through the same associated BS [27]. However, to offload the excessively loaded high-power BSs and to minimize the cumulative interference, various research works propose DL and UL decoupled (DUDe) access, where each UE is allowed to associate itself to different tier BSs in DL and UL, for improving the system's performance [27]–[29]. Traditionally, DUDe access assumes the same pathloss exponents across all the tiers to investigate the performance of multi-tier T-HCNs [27]–[30]. However, this may not be a reasonable assumption for AT-HCNs and is regarded as unrealistic, therefore, it is not practical to consider the same pathloss exponents across all the tiers in AT-HCNs.

In [31]–[34], decoupled-enabled regions are shown to be viable geographical regions for leveraging the benefits of DUDe access, where the UE receives maximum signal strength from the high power BS in DL while in the UL, maximum signal strength is received at the low power BS from the typical UE. If a decoupled access is permitted, then the UEs in the decoupled-enabled region are associated with DL and UL for the high- and low-power BSs, respectively. However, without a decoupled access, the UEs residing in the decoupled-enabled regions will be associated with DL and UL for the same BS. In [34], the SE of the T-HCNs is investigated for the decoupled-enabled region in terms of Fox H-function, where the authors showed that the performance of the decoupled access is higher than the non-decoupled access. Fox H-function enables obtaining closed-form solutions for complex infinite integrals. The implementation aspects of uni-variate and bi-variate Fox H-function are studied in [35] and [36], respectively.

B. MAJOR CONTRIBUTIONS

Without decoupling, [14] presents an analytical framework of A-HCNs, which is similar to the conventional T-HCNs. The authors modeled the spatial distribution of the UEs as an independent HPPP and derived the outage probability of the typical UEs by considering the same value for pathloss exponents across all the tiers (multiple tier networks). However, the HPPP based modeling cannot accurately represent the network interference for such clustered environments. Furthermore, the assumption of considering the same pathloss exponent across all the tiers of a multi-tier A-HCNs can be regarded as an oversimplified approach.

This work focuses on the performance of decoupled access for AT-HCNs with clustered users by considering different pathloss exponents for multiple-tiers. To the best of the authors' knowledge, this is the first research effort to investigate the scope of decoupled access for AT-HCNs. Compared to the research work in [14], [27], [34], the main contributions of this work can be listed as follows:

- The association probabilities of the typical UE are derived in terms of the uni-variate Fox H-function. This enables the analysis for more generalized use-cases with different pathloss exponents in different tiers.
- Closed-form analytical expressions for the coverage-, spectral-, and energy-efficiency of decoupled and the non-decoupled access schemes are derived by employing the bi-variate Fox H-function.
- Using the developed analytical framework, performance analysis of AT-HCNs for variations in density of low-power BSs and the number of clusters is conducted.

Extensive simulations are conducted to establish the validity of the proposed analytical framework and derived expressions. Furthermore, the conducted analysis also indicates a significant performance improvement offered by the decoupled access and provide quantitative insights on the pros-and-cons of such an access strategy.

C. PAPER ORGANIZATION

The organization of this paper is as follows. Section II describes the system model of AT-HCNs. In Section III, the clustered interference is investigated. Section IV derives the UL coverage, SE, and EE while, Section V describes network slicing in AT-HCNs followed by Section VI, which includes the main results and discussion. Finally, the paper is concluded in Section VII.

II. SYSTEM MODEL

We consider a two-tier AT-HCN as shown in Fig. 1. The BSs in the k-th tier are distributed as an independent HPPP Φ_k i.e., $k \in \{H, L\}$, where H and L represent high power BS and low power BS, respectively. The BSs are further segregated as aerial or terrestrial using $q_k \in [0, 1]$, where $q_k = 1$ indicates that in the k-th tier all the BSs are terrestrial[1]. In our model, the density, antenna height, transmit power, and pathloss exponent of the k-th tier BSs is represented by λ_k, h_k, P_k, and α_k, respectively.

We model clustering scenario for AT-HCNs, where UEs are distributed according to an MCP [21], [37]. The MCP consists of parent nodes and child nodes. The parent nodes with density λ_p, are modeled according to an independent HPPP, while the child nodes are independently and identically distributed around the parent nodes in a circular cluster of radius r_p. The parent nodes themselves are not included in the MCP. The density of UEs in the region of interest is given as $\lambda_U = \lambda_p \bar{c}$, where $\bar{c}$ is the average number of child nodes per cluster. The probability density function (pdf) of the uniformly distributed UEs with distance $\| y \|$ in a cluster is

$$f_M(y) = \frac{1}{\pi r_p^2}, \qquad \| y \| \leq r_p. \tag{1}$$

We also note that according to Slivnyak's Theorem (see, e.g., [38]) the distribution of the point process remains unchanged by placing a point at the origin. Therefore, for brevity and without loss of generality we consider a typical UE located at the origin $x_o = (0, 0, 0)$. The intended BS in the UL is referred to as a tagged BS. The Euclidean distance between the typical UE and the k-th tier tagged BS is given as $\| X_k \|$. The small scale fading between the UE and the BS is assumed to be an independent and Rayleigh, where the fading gain is modeled as $g_{X_k} \sim \exp(1)$.

For the successful detection of the received signal, the power transmitted by the UE, when associated to high and low power BS is Q_H and Q_L, respectively. Similar to [31], [34], we consider fixed transmit power of the UE to make the analysis of the Cases 1-4 (in Section III-A) less complex and to track the effect of varying Q_H and Q_L on the association probabilities of the derived use-cases.

[1]BS refers to both terrestrial and aerial BS, T-HCN refers to terrestrial HCN without aerial BSs, and A-HCN refers to aerial HCN without terrestrial BSs.

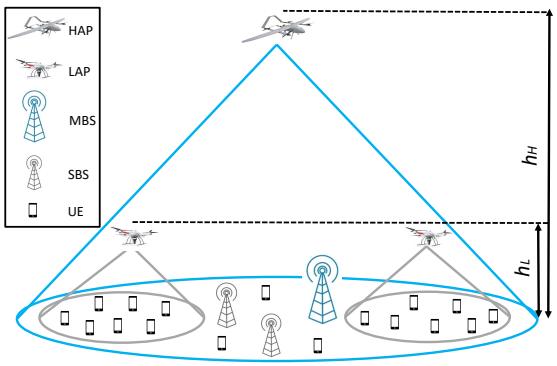

FIGURE 1: Illustration of a typical AT-HCN.

The average power received from the k-th tier BS at the typical UE is $\mathbb{E}\{S_k^{\mathrm{DL}}\} = P_k \parallel X_k \parallel^{-\alpha_k}$, where $\mathbb{E}\{.\}$ is statistical expectation. The average power received from the typical UE at the k-th tier BS is $\mathbb{E}\{S_k^{\mathrm{UL}}\} = Q_k \parallel X_k \parallel^{-\alpha_k}$. The additive Gaussian noise power at the receiver is σ^2 and τ is the received signal-to-interference-plus-noise ratio (SINR) threshold. Similar to the work of [21], [37], where the received UL SINR is characterized by the clustered users, we focus only on the UL SINR. Thus, the UL SINR of the k-th tier BS is

$$\mathrm{SINR}_{X_k}^{\mathrm{UL}} \triangleq \frac{Q_k g_{X_k} \parallel X_k \parallel^{-\alpha_k}}{\sum_{j \epsilon \Phi_I} Q_k g_{X_j} \parallel X_j - X_k \parallel^{-\alpha_k} + \sigma^2}. \tag{2}$$

We further define the interferes process, Φ_I, is an MCP with density $\lambda_I = \lambda_{I_p} \bar{c_I}$, where λ_{I_p} is the density of interfering parent nodes. The average number of the UEs taking part in the interference process is denoted by $\bar{c_I}$. We further assume that $\lambda_U \geq (\lambda_H + \lambda_L)$, i.e., at least one UE is associated with each tier in the UL.

For easy reference possible DL and UL user association scenarios is provided in Table 1, followed by definitions of notations used in the expressions of Fox H-function in Table 2. We further provide a list of parameters, their descriptions and their values used in our simulations in Table 3.

III. INTERFERENCE ANALYSIS

To obtain the interference in UL and DL, we need to investigate the association probabilities, and the distance distributions to the nearest tier BS.

TABLE 1: DL and UL user-association scenarios.

Association	DL	UL	Case
Coupled	High power BS	High power BS	1
Coupled	Low power BS	Low power BS	2
Decoupled	High power BS	Low power BS	3
Decoupled	Low power BS	High power BS	4

A. DL AND UL ASSOCIATION PROBABILITIES

The typical UE is associated with the high power BS in DL, if

$$P_H \parallel X_H \parallel^{-\alpha_H} > P_L \parallel X_L \parallel^{-\alpha_L},$$

otherwise, it is associated with the low power BS. Similarly, the typical UE is associated with the high power BS in UL, if

$$Q_H \parallel X_H \parallel^{-\alpha_H} > Q_L \parallel X_L \parallel^{-\alpha_L},$$

otherwise, it is associated with the low power BS.

The association of the typical UE to the k-th tier BS means that no BS from the other tier exists within a sphere with radius X_k. Therefore, $\mathbb{P}\{X_k > x\} = e^{-\pi\lambda_k x^2}$ [38] and the pdf of the distance of the typical UE to its nearest k-th tier BS is

$$f_{X_k}(x) = 2\pi\lambda_k x e^{-\pi\lambda_k x^2}, \quad x \geq 0. \tag{3}$$

The typical UE is associated with the tagged BS based on the quality of received power in the DL and the UL as shown in Fig. 2. Hence, four possible cases are envisaged. Two of the possible cases are for the coupled association while the remaining two possible cases are for the decoupled association as shown in Table 1. The association of the typical UE in both DL and UL with the same tier BS is known as a coupled association whereas, the association of the typical UE in DL with one BS and in UL with another is referred to as the decoupled association. In the following, we investigate Cases 1-4.

1) Case 1: Coupled Association of DL & UL to the high power BS

The probability of the typical UE is being associated in both DL and UL with the high power BS is

$$\mathcal{P}_{C_1} = \mathbb{P}\left\{P_H X_H^{-\alpha_H} > P_L X_L^{-\alpha_L} \; ; \; Q_H X_H^{-\alpha_H} > Q_L X_L^{-\alpha_L}\right\}.$$

Since $P_H > P_L$, the joint probability is reduced to $\mathbb{P}\{Q_H X_H^{-\alpha_H} > Q_L X_L^{-\alpha_L}\}$. Then the user association probability in terms of uni-variate Fox H-function is given as

$$\mathcal{P}_{C_1} = \mathbb{P}\left\{X_H < \left(\frac{Q_H}{Q_L}\right)^{\frac{1}{\alpha_H}} X_L^{\frac{\alpha_L}{\alpha_H}}\right\}$$

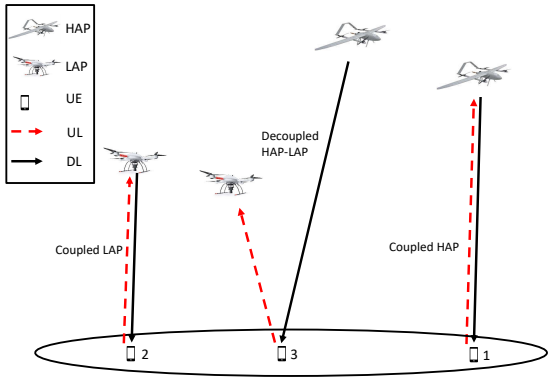

FIGURE 2: Possible DL and UL user-association scenarios in A-HCNs. UEs marked by 1, 2 and 3 represent Case 1, 2 and 3, respectively.

$$\stackrel{a}{=} 1 - 2\pi\lambda_L \int_0^\infty \exp\left\{-\pi\lambda_H \left(\frac{Q_H}{Q_L}\right)^{\frac{2}{\alpha_H}} x^{\frac{2\alpha_L}{\alpha_H}} - \pi\lambda_L x^2\right\} dx$$

$$\stackrel{b}{=} 1 - 2\pi\lambda_L \int_0^\infty \left(\frac{\alpha_H}{2\alpha_L} \mathcal{H}_{0,1}^{1,0}\left[\Psi_1 x \middle| \begin{matrix}(-,-)\\ \left(0, \frac{\alpha_H}{2\alpha_L}\right)\end{matrix}\right]\right.$$

$$\left. \cdot \frac{1}{2} \mathcal{H}_{0,1}^{1,0}\left[\Psi_2 x \middle| \begin{matrix}(-,-)\\ \left(0, \frac{1}{2}\right)\end{matrix}\right] x\right) dx$$

$$\stackrel{c}{=} 1 - \frac{\alpha_H}{2\alpha_L} \mathcal{H}_{1,1}^{1,1}\left[\Psi_a \middle| \begin{matrix}\left(0, \frac{1}{2}\right)\\ \left(0, \frac{\alpha_H}{2\alpha_L}\right)\end{matrix}\right], \tag{4}$$

where $\stackrel{a}{=}$ is obtained using (3), while $\stackrel{b}{=}$ is obtained using uni-variate Fox H-function as defined in (5) with parameters $m_1 = 1, n_1 = 0, v_1 = 0$, and $w_1 = 1$, and using (2.9.4) of [39]. In (5), $\Gamma(t) = \int_0^\infty s^{t-1} e^{-s} ds$, γ can be any real or complex number not equal to zero and an empty product is considered as unity. Further in (5), m_1, n_1, v_1, and w_1 are positive integers so that, $1 \leqslant m_1 \leqslant w_1, 0 \leqslant n_1 \leqslant v_1, A_j > 0, B_j > 0$ and a_j, b_j are complex numbers, and $\mathfrak{C}$ is a is a certain contour separating the poles of the two factors in the numerator. Finally, in (4), $\stackrel{c}{=}$ is obtained by integrating the product of two uni-variate Fox H-functions given in (2.8.4) of [39].

2) Case 2: Coupled Association of DL & UL to the low power BS

The DL and UL coupled association probability of the typical UE with the low power BS is

$$\mathcal{P}_{C_2} = \mathbb{P}\left\{P_L X_L^{-\alpha_L} \geq P_H X_H^{-\alpha_H} \; ; \; Q_L X_L^{-\alpha_L} \geq Q_H X_H^{-\alpha_H}\right\}.$$

$$\mathcal{H}_{v_1,w_1}^{m_1,n_1}(\gamma) \triangleq \mathcal{H}_{v_1,w_1}^{m_1,n_1}\left[\gamma\middle|\begin{matrix}(a_1,A_1),...,(a_{v_1},A_{v_1})\\(b_1,B_1),...,(b_{w_1},B_{w_1})\end{matrix}\right] = \frac{1}{2\pi\iota}\oint_{\mathfrak{C}}\frac{\Pi_{j=1}^{m_1}\Gamma(b_j+B_js)\Pi_{j=1}^{m_1}\Gamma(1-a_j+A_js)}{\Pi_{j=n_1+1}^{v_1}\Gamma(a_j+A_js)\Pi_{j=m_1+1}^{w_1}\Gamma(1-b_j+B_js)}\gamma^{-s}d\gamma, \quad (5)$$

TABLE 2: Definitions of notations used in the expressions of Fox H-function [34].

Notations	Definitions
Ψ_H	$\frac{\sigma^2(\tau)^{1/\alpha_H}}{Q_H^{1/\alpha_H}}$
Ψ_L	$\frac{\sigma^2(\tau)^{1/\alpha_L}}{Q_L^{1/\alpha_L}}$
$\bar{\Psi}_H$	$\frac{\sigma^2(e^t-1)^{1/\alpha_H}}{Q_H^{1/\alpha_H}}$
$\bar{\Psi}_L$	$\frac{\sigma^2(e^t-1)^{1/\alpha_L}}{Q_L^{1/\alpha_L}}$
Ψ_1	$(\sqrt{\pi\lambda_H})^{\alpha_H/\alpha_L}(Q_H/Q_L)^{1/\alpha_L}$
Ψ_2	$\sqrt{\pi\lambda_L}$
Ψ_3	$(\sqrt{\pi\lambda_H})^{\alpha_H/\alpha_L}(P_H/P_L)^{1/\alpha_L}$
Ψ_4	$(\sqrt{\pi\lambda_L})^{\alpha_L/\alpha_H}(P_L/P_H)^{1/\alpha_H}$
Ψ_5	$(\sqrt{\pi\lambda_L})^{\alpha_L/\alpha_H}(Q_L/Q_H)^{1/\alpha_H}$
Ψ_6	$\sqrt{\pi\lambda_H}$
Ψ_7	$\sqrt{\pi(\lambda_L+\Upsilon_L)}$
Ψ_8	$\sqrt{\pi(\lambda_H+\Upsilon_H)}$
Ψ_a	$\frac{\Psi_1}{\Psi_2}$
Ψ_b	$\frac{\Psi_3}{\Psi_2}$

Similar to Case 1, the joint probability is reduced to $X_L^{-\alpha_L} \geq \frac{P_H}{P_L}X_H^{-\alpha_H}$. Then, the user association probability is obtained by following the same steps as in Case 1:

$$\mathcal{P}_{C_2} = \mathbb{P}\left\{X_H > \left(\frac{P_H}{P_L}\right)^{\frac{1}{\alpha_H}} X_L^{\frac{\alpha_L}{\alpha_H}}\right\}$$
$$= 2\pi\lambda_L\int_0^\infty \exp\left\{-\pi\lambda_H\left(\frac{P_H}{P_L}\right)^{\frac{2}{\alpha_H}} x^{\frac{2\alpha_L}{\alpha_H}} - \pi\lambda_L x^2\right\}dx$$
$$= 2\pi\lambda_L\int_0^\infty \left(\frac{\alpha_H}{2\alpha_L}\mathcal{H}_{0,1}^{1,0}\left[\Psi_3 x\middle|\begin{matrix}(-,-)\\(0,\frac{\alpha_H}{2\alpha_L})\end{matrix}\right]\right.$$
$$\left.\cdot\frac{1}{2}\mathcal{H}_{0,1}^{1,0}\left[\Psi_2 x\middle|\begin{matrix}(-,-)\\(0,\frac{1}{2})\end{matrix}\right]x\right)dx$$
$$= \frac{\alpha_H}{2\alpha_L}\mathcal{H}_{1,1}^{1,1}\left[\Psi_b\middle|\begin{matrix}(0,\frac{1}{2})\\(0,\frac{\alpha_H}{2\alpha_L})\end{matrix}\right]. \quad (6)$$

3) Case 3: Decoupled Association of DL to the high power BS and UL to the low power BS

The probability that the typical UE is being associated with the high power BS in the DL and with the low power BS in the UL (see, Fig. 2) is

$$\mathcal{P}_{C_3}=\mathbb{P}\left\{P_H X_H^{-\alpha_H} > P_L X_L^{-\alpha_L}\ ;\ Q_H X_H^{-\alpha_H} \leq Q_L X_L^{-\alpha_L}\right\}.$$

Since $P_H > P_L$, the joint event is expressed as $\frac{P_L}{P_H}X_L^{-\alpha_L} < X_H^{-\alpha_H} \leq \frac{Q_L}{Q_H}X_L^{-\alpha_L}$. The user association probability is then obtained by following the same line of argument as of Case 1 as

$$\mathcal{P}_{C_3} = \mathbb{P}\left\{X_H < \left(\frac{P_H}{P_L}\right)^{\frac{1}{\alpha_H}} X_L^{\frac{\alpha_L}{\alpha_H}}\right\} -$$
$$\mathbb{P}\left\{X_H < \left(\frac{Q_H}{Q_L}\right)^{\frac{1}{\alpha_H}} X_L^{\frac{\alpha_L}{\alpha_H}}\right\}$$
$$= \int_0^\infty \left(1-\exp\left\{-\pi\lambda_H\left(P_H/P_L\right)^{2/\alpha_H} x^{\frac{2\alpha_L}{\alpha_H}}\right\} -\right.$$
$$\left.\left(1-\exp\left\{-\pi\lambda_H\left(Q_H/Q_L\right)^{2/\alpha_H} x^{\frac{2\alpha_L}{\alpha_H}}\right\}\right)\right) f_{X_L}(x)dx$$
$$= 1 - 2\pi\lambda_L\int_0^\infty \left(\frac{\alpha_H}{2\alpha_L}\mathcal{H}_{0,1}^{1,0}\left[\Psi_3 x\middle|\begin{matrix}(-,-)\\(0,\frac{\alpha_H}{2\alpha_L})\end{matrix}\right]\right.$$
$$\left.\cdot\frac{1}{2}\mathcal{H}_{0,1}^{1,0}\left[\Psi_2 x\middle|\begin{matrix}(-,-)\\(0,\frac{1}{2})\end{matrix}\right]x\right)dx - (1-2\pi\lambda_L$$
$$\int_0^\infty\left(\frac{\alpha_H}{2\alpha_L}\mathcal{H}_{0,1}^{1,0}\left[\Psi_1 x\middle|\begin{matrix}(-,-)\\(0,\frac{\alpha_H}{2\alpha_L})\end{matrix}\right]\frac{1}{2}\mathcal{H}_{0,1}^{1,0}\left[\Psi_2 x\middle|\begin{matrix}(-,-)\\(0,\frac{1}{2})\end{matrix}\right]x\right)dx\Bigg)$$
$$= \frac{\alpha_H}{2\alpha_L}\left(\mathcal{H}_{1,1}^{1,1}\left[\Psi_a\middle|\begin{matrix}(0,\frac{1}{2})\\(0,\frac{\alpha_H}{2\alpha_L})\end{matrix}\right] - \mathcal{H}_{1,1}^{1,1}\left[\Psi_b\middle|\begin{matrix}(0,\frac{1}{2})\\(0,\frac{\alpha_H}{2\alpha_L})\end{matrix}\right]\right). \quad (7)$$

4) Case 4: Decoupled Association of DL to the low power BS and UL to the high power BS

The probability that the typical UE associates with low power BS in DL and high power BS in UL is

$$\mathcal{P}_{C_4}=\mathbb{P}\left\{P_H X_H^{-\alpha_H}\leq P_L X_L^{-\alpha_L}\ ;\ Q_H X_H^{-\alpha_H}> Q_L X_L^{-\alpha_L}\right\}.$$

The simplified association probability is

$$\mathcal{P}_{C_4}=\mathbb{P}\left\{\frac{P_L}{P_H}X_L^{-\alpha_L}\geq X_H^{-\alpha_H}>\frac{Q_L}{Q_H}X_L^{-\alpha_L}\right\}=0. \quad (8)$$

Since $P_H > P_L$, it is straight forward to show that it is practically not possible for the typical UE to be associated with a low power BS in DL and a high power BS in UL.

B. DISTANCE TO THE NEAREST BS

Here, we derive the distance between the typical UE and the tagged k-th tier BS residing in the decoupled-enabled region for both the decoupled and non-decoupled access schemes. This distance will then be used in characterizing the UL interference. Since for the decoupled access, the tagged BS is the low power BS while for the non-decoupled access, the tagged BS is the high power BS. Therefore, the distance distribution of the typical UE to a tagged BS is different for both the schemes. The complementary cumulative distribution function (CCDF) of the distance to the tagged low power BS $F_{X_L}^{c_3}(.)$, in the decoupled access scheme is thus given by:

$$F_{X_L}^{c_3}(x)=\mathbb{P}\left\{X_L>x\mid \frac{P_L}{P_H}X_L^{-\alpha_L}<X_H^{-\alpha_H}\leq\frac{Q_L}{Q_H}X_L^{-\alpha_L}\right\},$$
$$\overset{a}{=}\int_x^\infty\left(\exp\left\{-\pi\lambda_H\left(\frac{Q_H}{Q_L}\right)^{\frac{2}{\alpha_H}}x^{\frac{2\alpha_L}{\alpha_H}}\right\}-\exp\left\{-\pi\lambda_H\left(\frac{P_H}{P_L}\right)^{\frac{2}{\alpha_H}}x^{\frac{2\alpha_L}{\alpha_H}}\right\}\right)\frac{f_{X_L}(x)dx}{\mathcal{P}_{C_3}}, \quad (9)$$

where 3 in the superscript represents analysis of the Case 3 and $\mathcal{P}_{C_3}$ is the association probability of the decoupled UEs given in (7). Then, $\overset{a}{=}$ is obtained by applying Bayes rule.

The pdf of the distance between the typical UE placed in the decoupled-enabled region and the tagged low power BS is

$$f_{X_L}^{(3)}(x)=\frac{d\left(1-F_{X_L}^{c_3}(x)\right)}{dx},$$
$$=\left(\exp\left\{-\pi\lambda_H\left(\frac{P_H}{P_L}\right)^{\frac{2}{\alpha_H}}x^{\frac{2\alpha_L}{\alpha_H}}\right\}-\exp\left\{-\pi\lambda_H\left(\frac{Q_H}{Q_L}\right)^{\frac{2}{\alpha_H}}x^{\frac{2\alpha_L}{\alpha_H}}\right\}\right)\frac{f_{X_L}(x)}{\mathcal{P}_{C_3}}. \quad (10)$$

Similarly, following the same line of argument, the pdf of the distance between the typical UE located in the decoupled-enabled region and the tagged high power BS is obtained as

$$f_{X_H}^{(3)}(x)=-\frac{dF_{X_H}^{c_3}(x)}{dx},$$
$$=\left(\exp\left\{-\pi\lambda_L\left(\frac{P_L}{P_H}\right)^{\frac{2}{\alpha_L}}x^{\frac{2\alpha_H}{\alpha_L}}\right\}-\exp\left\{-\pi\lambda_L\left(\frac{Q_L}{Q_H}\right)^{\frac{2}{\alpha_L}}x^{\frac{2\alpha_H}{\alpha_L}}\right\}\right)\frac{f_{X_H}(x)}{\mathcal{P}_{C_3}}. \quad (11)$$

C. UPLINK INTERFERENCE

Here, we characterize the effect of UL interference in terms of Laplace Transform. Consider $\upsilon(x)=\mathcal{L}_I(.)$, then using [25], [40], the UL interference at a k-th tier BS is given by the probability generating function (PGFL), $G(\upsilon)$ and the conditional PGFL, $\zeta(\upsilon)$ and is expressed as

$$\zeta(\upsilon)=\mathbb{E}\left\{\Pi_{x\epsilon\Phi}\upsilon(x)\right\}$$
$$=G(\upsilon)\times\Omega, \quad (12)$$

where

$$\Omega\triangleq\exp\left\{-x_k^2\tau^{2/\alpha_k}\frac{2\pi\bar{c_I}}{\alpha_k r_p^2}\csc(2\pi/\alpha_k)\right\}. \quad (13)$$

The PGFL is obtained by setting the pathloss exponent $\alpha_k > 2$. Thus, the PGFL of the MCP distributed users in the k-th tier is given as

$$G(\upsilon)=\exp\left\{-\lambda_{I_p}\pi\tau^{2/\alpha_k}x_k^2\int_0^\infty\left(1-\exp\left\{\frac{-\bar{c_I}}{1+t^{\alpha_k/2}}\right\}\right)dt\right\}. \quad (14)$$

Then, the Laplace Transform of UL interference is obtained by substituting (13) and (14) in (12) as the following.

$$\mathcal{L}_I(x_k\tau)=\exp\left\{-x_k^2\tau^{2/\alpha_k}\frac{2\pi\bar{c_I}}{\alpha_k r_p^2}\csc(2\pi/\alpha_k)-\lambda_{I_p}\pi\tau^{2/\alpha_k}x_k^2\int_0^\infty\left(1-\exp\left\{\frac{-\bar{c_I}}{1+t^{\alpha_k/2}}\right\}\right)dt\right\}.$$

We further define

$$\aleph\triangleq\int_0^\infty\left(1-\exp\left\{\frac{-\bar{c_I}}{1+t^{\alpha_k/2}}\right\}\right)dt,$$
$$\Upsilon_k\triangleq\tau^{2/\alpha_k}\left(\frac{\alpha_k\lambda_{I_p}\aleph r_p^2+2\bar{c_I}\csc(2\pi/\alpha_k)}{\alpha_k r_p^2}\right),$$

thus $\mathcal{L}_I(x_k\tau)$ is further simplified by considering $s=x_k\tau$ to

$$\mathcal{L}_I(s)=\exp\{-\pi x_k^2\Upsilon_k\}. \quad (15)$$

IV. PERFORMANCE ANALYSIS

A. COVERAGE PROBABILITY

The UL coverage probability of the typical UE is defined as the probability that the tagged BS receives an SINR greater than the pre-defined threshold. The CCDF of SINR at the k-th tier BS corresponds to the UL coverage probability of the

typical UE and is given as

$$C \triangleq \mathbb{E}_{X_k}\left\{\mathbb{P}\{\mathrm{SINR}^{\mathrm{UL}}_{X_k} > \tau\}\right\}. \tag{16}$$

The UL coverage probability of the decoupled access at the tagged low power BS is defined as the probability that the tagged low power BS receives an SINR greater than the pre-defined threshold. Then, the UL coverage probability of the decoupled access is formulated as

$$C^D \triangleq \mathbb{E}_{X_L}\left\{\mathbb{P}\{\mathrm{SINR}^{\mathrm{UL}}_{X_L} > \tau\}\right\}. \tag{17}$$

The UL coverage performance of the decoupled access is derived in Proposition 1.

Proposition 1. *The UL coverage probability of the decoupled access with the MCP distributed users is*

$$C^D = \pi\lambda_L . \frac{\alpha_H}{2\alpha_L^2}\left(\frac{\sigma^2\tau}{Q_L}\right)^{\frac{-2}{\alpha_L}}\left(\hat{\mathcal{H}}\left(\frac{\Psi_1}{\Psi_L},\frac{\Psi_7}{\Psi_L}\right) - \hat{\mathcal{H}}\left(\frac{\Psi_3}{\Psi_L},\frac{\Psi_7}{\Psi_L}\right)\right). \tag{18}$$

Proof. See Appendix A. ∎

The UL coverage probability of the non-decoupled access at the tagged high power BS can be defined as the probability that the tagged high power BS receives an SINR greater than the pre-defined threshold. Therefore, the UL coverage probability of the non-decoupled access is formulated as

$$C^{ND} \triangleq \mathbb{E}_{X_H}\left\{\mathbb{P}\{\mathrm{SINR}^{\mathrm{UL}}_{X_H} > \tau\}\right\}. \tag{19}$$

The UL coverage performance of the non-decoupled access is derived in Proposition 2.

Proposition 2. *The UL coverage probability of the non-decoupled access with the MCP distributed users is*

$$C^{ND} = \pi\lambda_H . \frac{\alpha_L}{2\alpha_H^2}\left(\frac{\sigma^2\tau}{Q_H}\right)^{\frac{-2}{\alpha_H}}\left(\hat{\mathcal{H}}\left(\frac{\Psi_4}{\Psi_H},\frac{\Psi_8}{\Psi_H}\right) - \hat{\mathcal{H}}\left(\frac{\Psi_5}{\Psi_H},\frac{\Psi_8}{\Psi_H}\right)\right). \tag{20}$$

Proof. Following the same line of argument as in the proof of Proposition 1, for the non-decoupled access, exploiting (11), (15), and considering X_H as the tagged high power BS, it is straight forward to obtain the coverage probability of the non-decoupled access. ∎

B. SPECTRAL EFFICIENCY

The UL channel capacity of the typical UE associated with the k-th tier BS normalized by the channel bandwidth describes the SE (nats/Hz) and is given as

$$\mathrm{SE} \triangleq \mathbb{E}_{X_k}\left\{\ln\left(1+\mathrm{SINR}^{\mathrm{UL}}_{X_k}\right)\right\}. \tag{21}$$

The difference between decoupled and non-decoupled access depends upon the association of the UEs in Case 3 with the high- and low-power BSs, therefore, we focus on SE of Case 3 for the decoupled and non-decoupled access. Thus, the SE of the decoupled and non-decoupled access is given in Proposition 3 and Proposition 4, respectively.

Proposition 3. *The SE in the UL of the decoupled access with the MCP distributed users is*

$$\mathrm{SE}^D = \pi\lambda_L . \frac{\alpha_H}{2\alpha_L^2}\int_0^\infty \bar{\Psi_L}^{-2}\left(\hat{\mathcal{H}}\left(\frac{\Psi_1}{\bar{\Psi_L}},\frac{\Psi_7}{\bar{\Psi_L}}\right) - \hat{\mathcal{H}}\left(\frac{\Psi_3}{\bar{\Psi_L}},\frac{\Psi_7}{\bar{\Psi_L}}\right)\right) dt. \tag{22}$$

Proof. See Appendix B. ∎

Proposition 4. *The SE in the UL of the non-decoupled access with the MCP distributed users is*

$$\mathrm{SE}^{ND} = \pi\lambda_H . \frac{\alpha_L}{2\alpha_H^2}\int_0^\infty \bar{\Psi_H}^{-2}\left(\hat{\mathcal{H}}\left(\frac{\Psi_4}{\bar{\Psi_H}},\frac{\Psi_8}{\bar{\Psi_H}}\right) - \hat{\mathcal{H}}\left(\frac{\Psi_5}{\bar{\Psi_H}},\frac{\Psi_8}{\bar{\Psi_H}}\right)\right) dt. \tag{23}$$

Proof. Following the same line of argument as in the proof of Proposition 3 and considering X_H as the tagged BS, it is straight forward to obtain SE of the non-decoupled access. ∎

C. ENERGY EFFICIENCY

The UL EE is defined as the UL channel capacity of the typical UE associated with the k-th tier BS normalized by the system power consumption and is given as

$$\mathrm{EE} \triangleq \frac{B}{Q_k}\mathbb{E}_{X_k}\left\{\ln\left(1+\mathrm{SINR}^{\mathrm{UL}}_{X_k}\right)\right\}, \tag{24}$$

where the system bandwidth is B. Here, we focus power consumption during the communication process by neglecting the power consumption of the flight operation modules. Thus, UL EE of the decoupled and non-decoupled access for Case 3 is formulated as $\mathrm{EE}^D = \frac{B}{Q_L}\mathrm{SE}^D$ and $\mathrm{EE}^{\mathrm{ND}} = \frac{B}{Q_H}\mathrm{SE}^{\mathrm{ND}}$, respectively.

V. NETWORK SLICING IN AT-HCNS

Network slicing (NS) is one of the promising solutions to provide cost-effective flexible networks by providing optimized logical networks (i.e., slices) on a shared physical infrastructure via network function virtualization (NFV) and software-defined networking (SDN) [41], [42]. Each slice is tailored to increase the date rates and the QoS by reducing the operational complexity. Our system model focuses and exploits the radio access and can be operated in combination with the NS to optimize the data rates and the QoS in AT-HCNs.

The NS considers that the core network (CN) is logically sliced but the radio access network (RAN) is un-sliced in the 5G architecture [43]. The isolation of RAN and CN is the key feature in the design principle of the network slicing and thus,

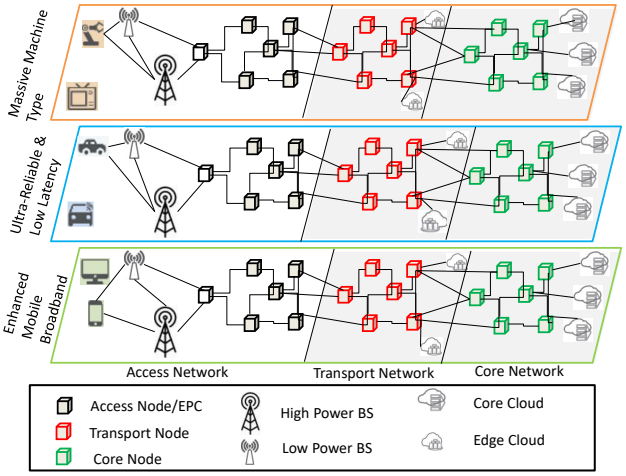

FIGURE 3: Network slicing supported in AT-HCNs.

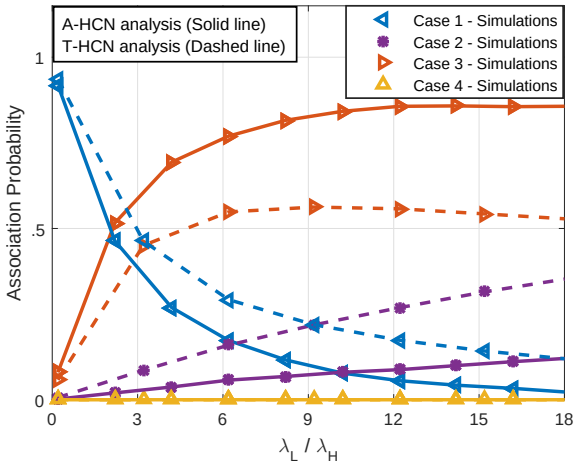

FIGURE 4: Effect of the density of low power BSs on the association probabilities for Cases 1–4.

allows the conventional RAN to operate in tandem with the 5G-supported sliced CN. The 3GPP developed support for the radio access of the conventional networks to be deployed in the 5G architecture and showed that the evolved packet core (EPC) is responsible for decoupling the data traffic between its associated nodes (e.g., high and low power BSs), to optimize the performance of the AT-HCNs (see Fig. 3) [44], [45]. Furthermore, our system model described for AT-HCNs can be implemented with NFV and SDN to consider decoupled control-/data plan by shaping the CN with minor modifications [46], [47].

VI. RESULTS AND DISCUSSION

This section presents results of a two-tier AT-HCN which are validated using $100,000$ Monte-Carlo runs. Unless stated otherwise, Table 3 summarizes the notations and the simulation parameters.

TABLE 3: Notations and Simulation Parameters

Notation	Description	Value
λ_H	High power BS density	$1/\pi 500^2$ m^{-2}
λ_L	Low power BS density	$5\lambda_H$
α_H	High power BS pathloss exponent	2.75
α_L	Low power BS pathloss exponent	3
P_H	High Power BS transmit power	46 dBm
P_L	Low power BS transmit power	30 dBm
h_H	High power BS height	300 m
h_L	Low power BS height	100 m
Q_H	Transmit power of the UE associated to high power BS	30 dBm
Q_L	Transmit power of the UE associated to low power BS	30 dBm
$\bar{c}$	Average UEs per cluster	20
λ_p	Parent clusters for UEs	$2/\pi 500^2$ m^{-2}
r_p	Cluster radius	40 m
σ^2	Noise power	-90 dBm
τ	SINR threshold	-20 dB
B	System bandwidth	20 MHz

Fig. 4 shows the association probability as a function of the density of the low power BSs. Considering Case 3 which is the focus of this work, it is observed that as the density of low power BS increases, larger number of the UEs prefer decoupled association. However, after a certain threshold, with the increase of the coupled low power BS association, decoupled association starts decreasing. This is because of the fact that with the further increase of low power BS density, larger number of UEs prefer coupled low power BS association. Further, for a given density, the association probability of the Case 3 UEs in A-HCNs is better than the T-HCNs because of the fact that the height of the aerial BSs is usually larger than the conventional BSs in T-HCNs. Thus, the distance-dependent pathloss between the typical UE and the tagged low power BS in A-HCNs is shorter than the distance-dependent pathloss between the typical UE and the tagged low power BS in T-HCNs, which results in the increase of received power and the corresponding association probability.

Fig. 5 shows that the coverage probability of both the access schemes, (i.e., decoupled and non-decoupled access) increases with the increase of low power BS density until a certain limit is surpassed. This is because of the fact that the distance-dependent pathloss between the typical UE and the tagged BS decreases which results in increasing the received SINR and the corresponding coverage probability. However, the coverage probability of the decoupled access is significantly higher than the non-decoupled access due to the shorter distance-dependent pathloss between the typical UE and the tagged low power BS than the tagged high power BS. The figure also shows that for a given density, the coverage probability of the A-HCNs is successful over the T-HCNs. This is because of the fact that the height of the LAPs is

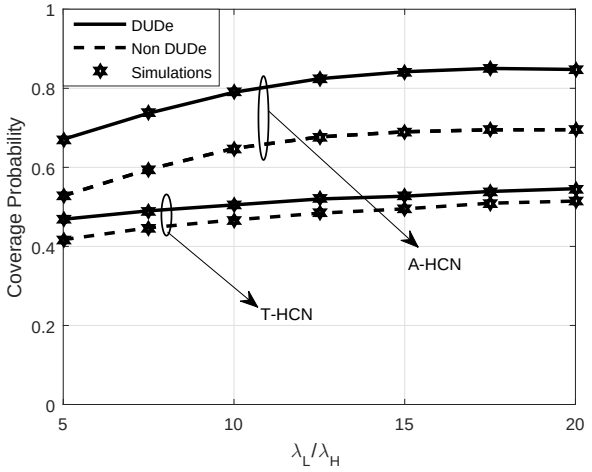

FIGURE 5: Coverage probability as a function of density of low power BSs.

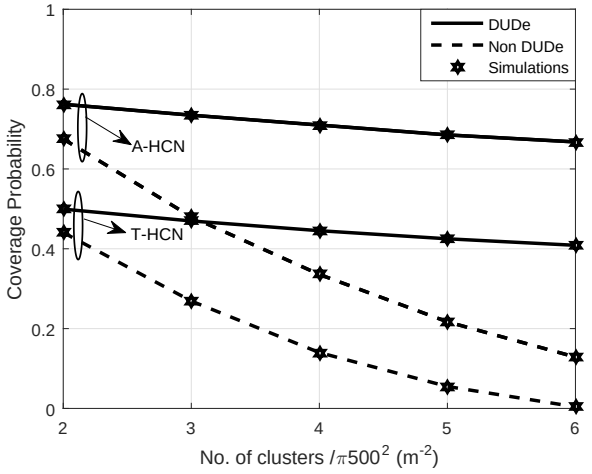

FIGURE 6: Coverage probability as a function of clustered-UEs, where $\lambda_L = 10\lambda_H$, $\alpha_H = 3$, and $\alpha_L = 3.25$.

mostly larger than the terrestrial BSs. Thus, the distance-dependent pathloss between the typical UE and the LAP is shorter than the distance-dependent pathloss between the typical UE and the low power terrestrial BS, which results in the increase of received power and the corresponding coverage probability.

Fig. 6 shows coverage probability as a function of the number of clustered-UEs. The coverage probability of the decoupled (DUDe labeled curve) and the non-decoupled (Non DUDe labeled curve) decreases with the increase of clusters because of the cumulative interference at the tagged BS increases which results in decreasing the received SINR and the corresponding coverage probability. The coverage probability of the decoupled access is significantly higher than the non-decoupled access because of the fact that the distance-dependent pathloss between the typical UE and the tagged low power BS is less than the tagged high power

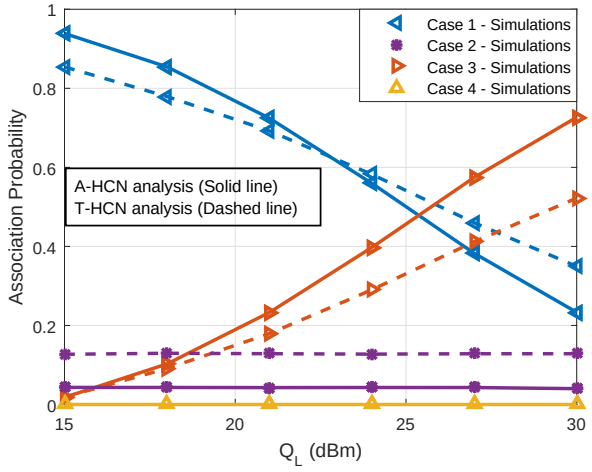

FIGURE 7: Association probability as a function of the UE's transmit power.

BS which results in increasing the received SINR and the corresponding coverage probability. Further, the coverage probability of the A-HCN is better than the T-HCN until a certain limit is surpassed because for a given density, more UEs follow decoupled association in the A-HCN than the T-HCN (see, Fig. 4). Thus, with the increase in the association probability of the decoupled UEs of the A-HCNs over the T-HCNs, more UEs can benefit the shorter distance-dependent pathloss between the typical UE and the low power BS of A-HCNs as compared to the low power BS of T-HCNs. As a result, a higher coverage probability of the A-HCNs is obtained, when comparing to the T-HCNs.

Fig. 7 shows the association probability as a function of the UE's transmit power. Considering Case 3 which is the focus of this work, it is observed that as the transmit power of the UE associated with the low power BS increases, larger number of the UEs prefer decoupled UE-association. This is because of the fact that with the increase of Q_L, more UEs are added in the decoupled-enabled region (i.e., Case 3) at the cost of the decrease in the coupled high power BS UE-association (i.e., Case 1). The association probability of the Case 3 UEs in the A-HCNs is better than the T-HCNs because of the fact that the height of the UAVs is usually larger than the conventional terrestrial BSs in T-HCNs. Thus, the distance-dependent pathloss between the typical UE and the LAPs is shorter than the low power BSs in T-HCNs, which results in the increase of received power and the corresponding association probability.

Fig. 8 shows the coverage probability as a function of the UE's transmit power. It is observed that the coverage probability of the decoupled and the non-decoupled access increases with the increase in Q_L. This is because of the fact that more UEs are added in the decoupled-enabled region with the increase in Q_L. It is also observed that the coverage performance of the decoupled access in both A-HCNs and T-HCNs is better than the non-decoupled access because the typical UE associates itself with the low power BS instead

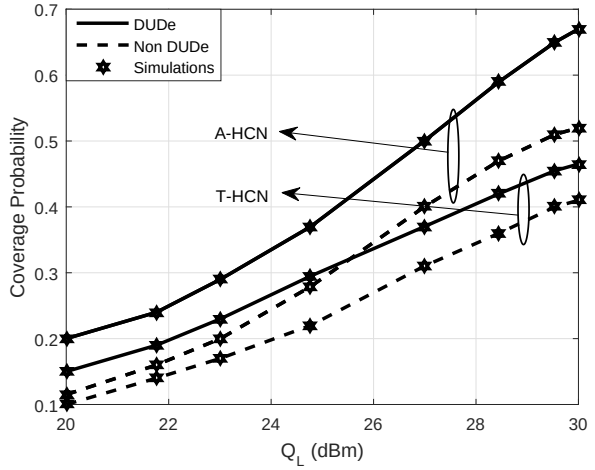

FIGURE 8: Coverage probability as a function of the UE's transmit power.

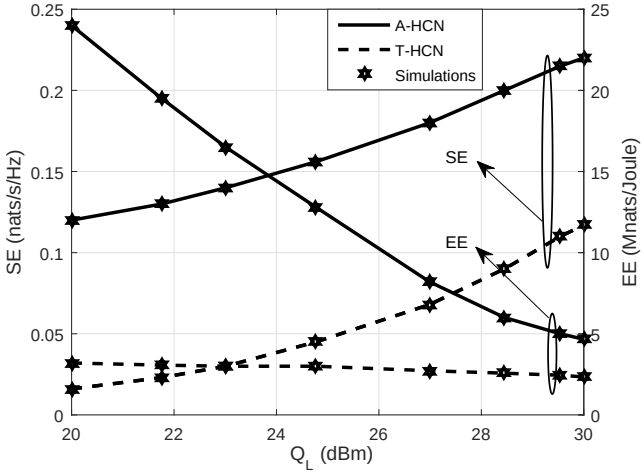

FIGURE 10: Effect of the UE's transmit power on the SE and EE. Other parameters are: $\alpha_H = 3.75$ and $\alpha_L = 4$.

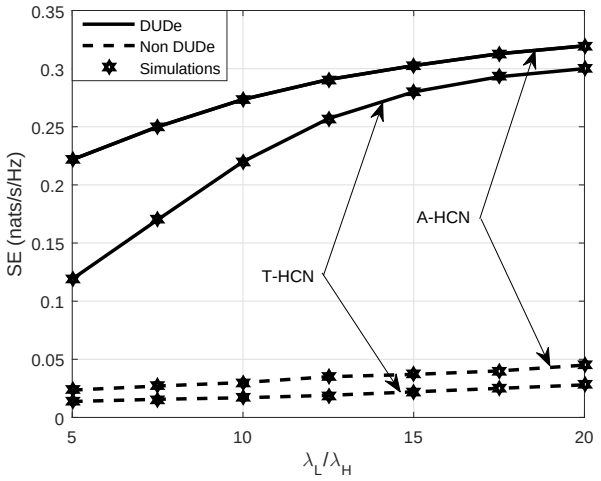

FIGURE 9: SE as a function of the density of low power BSs. Other parameters are: $\alpha_H = 3.75$ and $\alpha_L = 4$.

of the high power BS and the distance-dependent pathloss for the low power BS is shorter than the high power BS. As a result, the received SINR and the corresponding coverage probability increases. Further, the coverage probability of the Case 3 UEs in the A-HCNs is better than the T-HCNs because of the fact that the height of the LAPs is usually larger than the terrestrial BSs which results in the shorter distance-dependent pathloss between the typical UE and the LAP when comparing to the terrestrial BSs and thus an increase in the received SINR and the coverage probability is observed.

Fig. 9 shows that the SE increases with increase of the low power BS density until a certain limit is surpassed because the distance-dependent pathloss between the typical UE and the tagged BS decreases which results in increasing the received SINR and the corresponding SE. The SE of the decoupled access is significantly higher than the non-decoupled access because the distance-dependent pathloss between the typical UE and the tagged low power BS is less than the tagged high power BS. It is observed that for a given density, the SE of the decoupled A-HCN is successful over the decoupled T-HCN because the association probability of the decoupled-UEs in A-HCN is larger than the T-HCN. Since, with the larger association probability of the decoupled-UEs in the A-HCNs, more UEs prefer decoupled access in the A-HCNs than the T-HCNs, therefore, the coverage probability of the A-HCNs is better than the T-HCNs.

The SE of the typical UE in the UL is largely dependent upon the UE's transmit power, BS density, and the pathloss exponent. Since, in our analysis, the typical UE transmits with the power of 30 dBm in the underlying environment by considering BS density, $\lambda_L = 5\lambda_H$ and pathloss exponents, $\alpha_H = 3.75$ and $\alpha_L = 4$, therefore, the obtained SE is around 0.22 nats/s/Hz. With the given parameters, the UL SE of the typical UE in a clustered network may be considered less when comparing to the typical value of the SE, i.e., 1 bps/Hz = 0.693 nats/s/Hz [48], but, is in agreement with the UL SE obtained in [32] for a two-tier HCN with clustered UEs.

Fig. 10 shows SE and EE of the decoupled access as a function of the transmit power of the UE associated with the low power BS, (i.e., Q_L). It is observed that the SE improves by increasing Q_L because more UEs are added in the decoupled-enabled region with the increase in Q_L. Thus, the association probability and the corresponding SE increases. Further, the EE degrades by increasing Q_L, however, the EE of the A-HCN is larger than the T-HCN. This is because, the probability of user-association for the decoupled-UEs in A-HCN is larger than the T-HCN. Furthermore, the SE and the EE of the A-HCNs is successful over the T-HCNs. This is because of the fact that the association probability of the decoupled-UEs in the A-HCNs is larger than the T-HCNs. Thus, more UEs can benefit the shorter distance-dependent pathloss between the typical UE and the low power BS of the A-HCNs than the T-HCNs which increases the SE and the EE of the decoupled access in A-HCNs over the T-HCNs.

$$\hat{\mathcal{H}}(x_1,y_1) \triangleq \hat{\mathcal{H}}\left[\left.\begin{matrix}\begin{pmatrix}m_1,n_1\\v_1,w_1\end{pmatrix}\\\begin{pmatrix}m_2,n_2\\v_2,w_2\end{pmatrix}\\\begin{pmatrix}m_3,n_3\\v_3,w_3\end{pmatrix}\end{matrix}\right|\begin{matrix}\begin{pmatrix}a_{v_1};\alpha_{v_1},A_{v_1}\\b_{w_1};\beta_{w_1},B_{w_1}\end{pmatrix}\\\begin{pmatrix}c_{v_2};r_{v_2}\\d_{w_2};\delta_{w_2}\end{pmatrix}\\\begin{pmatrix}e_{v_3},E_{v_3}\\f_{w_3},F_{w_3}\end{pmatrix}\end{matrix}\right](x_1,y_1) \tag{25}$$
$$= \left(\frac{1}{2\pi\iota}\right)^2 \int_{\mathfrak{C}_1}\int_{\mathfrak{C}_2} \frac{\Pi_{j=1}^{n_1}\Gamma(1-a_j+\alpha_j s+A_j t)}{\Pi_{j=1}^{w_1}\Gamma(1-b_j+\beta_j s+B_j t)\Pi_{j=n_1+1}^{v_1}\Gamma(a_j-\alpha_j s-A_j t)}$$
$$\times \frac{\Pi_{j=1}^{m_2}\Gamma(d_j-\delta_j s)\Pi_{j=1}^{n_2}\Gamma(1-c_j+r_j s)}{\Pi_{j=n_2+1}^{v_2}\Gamma(c_j-r_j s)\Pi_{j=m_2+1}^{w_2}\Gamma(1-d_j+\delta_j s)} \times \frac{\Pi_{j=1}^{m_3}\Gamma(f_j-F_j s)\Pi_{j=1}^{n_3}\Gamma(1-e_j+E_j s)}{\Pi_{j=n_3+1}^{v_3}\Gamma(e_j-E_j s)\Pi_{j=m_3+1}^{w_3}\Gamma(1-f_j+F_j s)} x_1^s y_1^t dx_1 dy_1$$

VII. CONCLUSION

In this paper, we investigated the performance of AT-HCNs system with clustered traffic and obtained coverage probability, SE, and EE. We assumed that the high and low power BSs were spatially distributed according to an HPPP, and the UEs were distributed according to an MCP. We then obtained the association probabilities of the coupled and decoupled BSs for different pathloss exponents and then obtained closed-form expression of coverage probability, SE, and EE based on Fox H-function. The obtained results suggested that the performance of decoupled access is significantly higher than the non-decoupled access and that the decoupling of A-HCNs is successful over the T-HCNs for a given density of the aerial BSs.

APPENDIX A PROOF OF PROPOSITION 1

At the decoupled-enabled region, the UEs are associated with a low power BS in the decoupled access. This is because the distance-dependent pathloss between the typical UE and the low power BS is less than that of the high power BS. Thus, by focusing Case 3, the UL coverage probability with the decoupled access is derived as

$$C^D \triangleq \mathbb{E}\left\{\mathbb{P}\{\text{SINR}_{X_L}^{\text{UL}} > \tau | X_L\}\right\}$$
$$= \int_0^\infty \mathbb{P}\{\text{SINR}_{X_L}^{\text{UL}} > \tau\} f_{X_L}^{(3)}(x)dx$$
$$\overset{a}{=} \int_0^\infty \mathbb{P}\left\{\frac{Q_L g_{X_L} \parallel X_L \parallel^{-\alpha_L}}{\sum_{j\epsilon\Phi_I} Q_L g_{X_j} \parallel X_j - X_L\parallel^{-\alpha_L} + \sigma^2} > \tau\right\} \times f_{X_L}^{(3)}(x)dx$$
$$\overset{b}{=} \int_0^\infty \mathbb{P}\left\{g_{X_L} > \frac{\tau x^{\alpha_L}}{Q_L}\left(\sigma^2 + I\right)\right\} f_{X_L}^{(3)}(x)dx$$
$$\overset{c}{=} \int_0^\infty \exp\left(\frac{-\tau x^{\alpha_L}\sigma^2}{Q_L}\right)\mathbb{E}\left\{\exp\left(\frac{-\tau x^{\alpha_L} I}{Q_L}\right)\right\} f_{X_L}^{(3)}(x)dx$$
$$\overset{d}{=} \int_0^\infty \exp\left(\frac{-\tau\sigma^2 x^{\alpha_L}}{Q_L}\right)\mathcal{L}_I(s) f_{X_L}^{(3)}(x)dx$$
$$\overset{e}{=} 2\pi\lambda_L \int_0^\infty x \frac{1}{\alpha_L}\mathcal{H}_{0,1}^{1,0}\left[\Psi_L x\left|\begin{matrix}(-,-)\\\left(0,\frac{1}{\alpha_L}\right)\end{matrix}\right.\right]$$
$$\cdot\left(\frac{\alpha_H}{2\alpha_L}\mathcal{H}_{0,1}^{1,0}\left[\Psi_1 x\left|\begin{matrix}(-,-)\\\left(0,\frac{\alpha_H}{2\alpha_L}\right)\end{matrix}\right.\right] - \frac{\alpha_H}{2\alpha_L}\mathcal{H}_{0,1}^{1,0}\left[\Psi_3 x\left|\begin{matrix}(-,-)\\\left(0,\frac{\alpha_H}{2\alpha_L}\right)\end{matrix}\right.\right]\right)$$
$$\cdot\frac{1}{2}\mathcal{H}_{0,1}^{1,0}\left[\Psi_7 x\left|\begin{matrix}(-,-)\\\left(0,\frac{1}{2}\right)\end{matrix}\right.\right]dx$$
$$\overset{f}{=} 2\pi\lambda_L\Psi_L^{-2}\left(\hat{\mathcal{H}}\left[\left.\begin{matrix}\begin{pmatrix}0,1\\1,0\end{pmatrix}\\\begin{pmatrix}1,0\\0,1\end{pmatrix}\\\begin{pmatrix}1,0\\0,1\end{pmatrix}\end{matrix}\right|\begin{matrix}\left(1-\frac{2}{\alpha_L};\frac{1}{\alpha_L},\frac{2}{\alpha_L}\right)\\-;-,-\\\left(-,-\\0,\frac{\alpha_H}{2\alpha_L}\right)\\\left(-,-\\0,\frac{1}{2}\right)\end{matrix}\right](\frac{\Psi_1}{\Psi_L},\frac{\Psi_7}{\Psi_L})\right.$$
$$\left.-\hat{\mathcal{H}}\left[\left.\begin{matrix}\begin{pmatrix}0,1\\1,0\end{pmatrix}\\\begin{pmatrix}1,0\\0,1\end{pmatrix}\\\begin{pmatrix}1,0\\0,1\end{pmatrix}\end{matrix}\right|\begin{matrix}\left(1-\frac{2}{\alpha_L};\frac{1}{\alpha_L},\frac{2}{\alpha_L}\right)\\-;-,-\\\left(-,-\\0,\frac{\alpha_H}{2\alpha_L}\right)\\\left(-,-\\0,\frac{1}{2}\right)\end{matrix}\right](\frac{\Psi_3}{\Psi_L},\frac{\Psi_7}{\Psi_L})\right]\right), \tag{26}$$

where $\overset{a}{=}$ is obtained by considering tagged BS as low power BS and substituting SINR from (2), $\overset{b}{=}$ follows by assuming $I = \sum_{j\epsilon\Phi_I} Q_L g_{X_j} \|X_j - X_L\|^{-\alpha_L}$, $\overset{c}{=}$ follows by exploiting the exponentially distributed Rayleigh fading gains and $\overset{d}{=}$ follows by the definition of Laplace Transform of interference as $\mathcal{L}_I(s) = \mathbb{E}\left\{e^{-Is}\right\}$, and $\overset{e}{=}$ is obtained using (2.9.4) in [39]. Function $\hat{\mathcal{H}}[-|-|-]$ is a bi-variate Fox H-Function as defined in [49] (see, (25)), where $\mathfrak{C}_1$ and $\mathfrak{C}_2$ are defined similar to $\mathfrak{C}$ in (5) and $m_1, n_1, v_1, w_1, m_2, n_2, v_2, w_2, m_3, n_3, v_3$, and w_3 are positive integers so that $m_1 = 0; v_1 \geqslant n_1 \geqslant 0; v_2 \geqslant n_2 \geqslant 0; v_3 \geqslant n_3 \geqslant 0; w_1 \geqslant 0; w_2 \geqslant m_2 \geqslant 0; w_3 \geqslant m_3 \geqslant 0$, and $\alpha_j, \beta_j, r_j, \delta_j, E_j, F_j, A_j$, and B_j are positive numbers. Finally, $\overset{f}{=}$ is obtained using (2.3) in [49].

APPENDIX B PROOF OF PROPOSITION 3

Consider a random variable X_L as the distance between the typical UE and the tagged low power BS. Similar to [48], the SE is derived by averaging taken over the spatial location and the fading. By focusing Case 3, the UL SE with the decoupled access is derived as

$$\begin{aligned}
\mathrm{SE}^D &= \mathcal{P}_{C_3}\int_0^\infty\int_0^\infty \mathbb{P}\left\{\mathrm{SINR}_{X_L}^{\mathrm{UL}} > e^t-1\right\}dxdt \\
&\overset{a}{=} \mathcal{P}_{C_3}\int_0^\infty\int_0^\infty \mathbb{P}\left\{h_{X_L} > x^{\alpha_L}\left(\frac{\sigma^2}{Q_L}+I\right)(e^t-1)\right\} \\
&\quad\times f_{X_L}^{(3)}(x)dxdt \\
&\overset{b}{=} \mathcal{P}_{C_3}\int_0^\infty\int_0^\infty \mathbb{E}\left\{h_{X_L} > e^{-x^{\alpha_L}\left(\frac{\sigma^2}{Q_L}+I\right)(e^t-1)}\right\} f_{X_L}^{(3)}(x)dxdt \\
&\overset{c}{=} \mathcal{P}_{C_3}\int_0^\infty\int_0^\infty e^{-\frac{x^{\alpha_L}\sigma^2(e^t-1)}{Q_L}}\mathcal{L}_I(\bar{s})f_{X_L}^{(3)}(x)dxdt \\
&\overset{d}{=} 2\pi\lambda_L\int_0^\infty\int_0^\infty x\frac{1}{\alpha_L}\mathcal{H}_{0,1}^{1,0}\left[\bar{\Psi}_L x\middle|\begin{pmatrix}(-,-)\\ \left(0,\frac{1}{\alpha_L}\right)\end{pmatrix}\right] \\
&\quad\cdot\left(\frac{\alpha_H}{2\alpha_L}\mathcal{H}_{0,1}^{1,0}\left[\Psi_1 x\middle|\begin{pmatrix}(-,-)\\ \left(0,\frac{\alpha_H}{2\alpha_L}\right)\end{pmatrix}\right]-\frac{\alpha_H}{2\alpha_L}\mathcal{H}_{0,1}^{1,0}\left[\Psi_3 x\middle|\begin{pmatrix}(-,-)\\ \left(0,\frac{\alpha_H}{2\alpha_L}\right)\end{pmatrix}\right]\right) \\
&\quad\cdot\frac{1}{2}\mathcal{H}_{0,1}^{1,0}\left[\Psi_7 x\middle|\begin{pmatrix}(-,-)\\ \left(0,\frac{1}{2}\right)\end{pmatrix}\right]dxdt \\
&\overset{e}{=} 2\pi\lambda_L\int_0^\infty \bar{\Psi}_L^{-2}\left(\hat{\mathcal{H}}\left[\begin{matrix}\binom{0,1}{1,0}\\ \binom{1,0}{0,1}\\ \binom{1,0}{0,1}\end{matrix}\middle|\begin{matrix}\left(1-\frac{2}{\alpha_L};\frac{1}{\alpha_L},\frac{2}{\alpha_L}\right)\\ -;-,-\\ \binom{-,-}{0,\frac{\alpha_H}{2\alpha_L}}\\ \binom{-,-}{0,\frac{1}{2}}\end{matrix}\middle|\left(\frac{\Psi_1}{\bar{\Psi}_L},\frac{\Psi_7}{\bar{\Psi}_L}\right)\right]\right. \\
&\quad\left.-\hat{\mathcal{H}}\left[\begin{matrix}\binom{0,1}{1,0}\\ \binom{1,0}{0,1}\\ \binom{1,0}{0,1}\end{matrix}\middle|\begin{matrix}\left(1-\frac{2}{\alpha_L};\frac{1}{\alpha_L},\frac{2}{\alpha_L}\right)\\ -;-,-\\ \binom{-,-}{0,\frac{\alpha_H}{2\alpha_L}}\\ \binom{-,-}{0,\frac{1}{2}}\end{matrix}\middle|\left(\frac{\Psi_3}{\bar{\Psi}_L},\frac{\Psi_7}{\bar{\Psi}_L}\right)\right]\right)dt,
\end{aligned} \tag{27}$$

where $\overset{a}{=}$ is obtained by substituting the values of $\mathrm{SINR}_{X_L}^{\mathrm{UL}}$ while, $\overset{b}{=}$ is obtained due to the assumption of exponential distributed Rayleigh fading gains. In (27), $\overset{c}{=}$ is obtained by using Laplace Transform of interference as $\mathcal{L}_I(\bar{s})$, where $\bar{s} = x^{\alpha_L}(e^t-1)/Q_L$ and by using $(2.9.4)$ in [39]. Furthermore, $\overset{d}{=}$ is obtained by using (15) and $(2.9.4)$ in [39], while $\overset{e}{=}$ is obtained using (2.3) in [49].

REFERENCES

[1] I. Union, "IMT traffic estimates for the years 2020 to 2030," Report ITU-R M. 2370–0, ITU-R Radiocommunication Sector of ITU, 2015.

[2] S. J. Nawaz, S. K. Sharma, S. Wyne, M. N. Patwary, and M. Asaduzzaman, "Quantum machine learning for 6G communication networks: State-of-the-art and vision for the future," IEEE Access, vol. 7, pp. 46 317–46 350, 2019.

[3] J. G. Andrews, "Seven ways that HetNets are a cellular paradigm shift," IEEE Communications Magazine, vol. 51, no. 3, pp. 136–144, 2013.

[4] A. Fotouhi, H. Qiang, M. Ding, M. Hassan, L. G. Giordano, A. Garcia-Rodriguez, and J. Yuan, "Survey on UAV cellular communications: Practical aspects, standardization advancements, regulation, and security challenges," IEEE Communications Surveys & Tutorials, to be published.

[5] R. I. Bor-Yaliniz, A. El-Keyi, and H. Yanikomeroglu, "Efficient 3D placement of an aerial base station in next generation cellular networks," in Proc. of International Conference on Communications (ICC), 2016, pp. 1–5.

[6] O. S. Oubbati, M. Atiquzzaman, P. Lorenz, M. H. Tareque, and M. S. Hossain, "Routing in flying Ad Hoc networks: Survey, constraints, and future challenge perspectives," IEEE Access, vol. 7, pp. 81 057–81 105, 2019.

[7] S. Sekander, H. Tabassum, and E. Hossain, "Multi-tier drone architecture for 5G/B5G cellular networks: Challenges, trends, and prospects," IEEE Communications Magazine, vol. 56, no. 3, pp. 96–103, 2018.

[8] M. Khoshkholgh, K. Navaie, H. Yanikomerogluy, V. Leung, K. Shin et al., "Coverage performance of aerial-terrestrial HetNets," arXiv preprint arXiv:1902.08547, 2019.

[9] N. Panigrahi and S. S. Panigrahi, "Processing data acquired by a drone using a gis: Designing a size-, weight-, and power-constrained system," IEEE Consumer Electronics Magazine, vol. 7, no. 2, pp. 50–54, 2018.

[10] M. M. Azari, Y. Murillo, O. Amin, F. Rosas, M.-S. Alouini, and S. Pollin, "Coverage maximization for a poisson field of drone cells," in Proc. of 28th Annual International Symposium on Personal, Indoor, and Mobile Radio Communications (PIMRC), 2017, pp. 1–6.

[11] C. She, C. Liu, T. Q. Quek, C. Yang, and Y. Li, "UAV-assisted uplink transmission for ultra-reliable and low-latency communications," in Proc. of IEEE International Conference on Communications Workshops (ICC Workshops), 2018, pp. 1–6.

[12] Z. Yin, J. Li, M. Dingt, F. Shu, F. Song, Y. Qian, and D. Lopez-Perez, "Uplink performance analysis of UAV user equipments in dense cellular networks," in ICC 2019-2019 IEEE International Conference on Communications (ICC). IEEE, 2019, pp. 1–7.

[13] B. Galkin, J. Kibilda, and L. A. DaSilva, "Coverage analysis for low-altitude UAV networks in urban environments," in GLOBECOM 2017-2017 IEEE Global Communications Conference. IEEE, 2017, pp. 1–6.

[14] M. Helmy and H. Arslan, "Utilization of aerial heterogeneous cellular networks: Signal-to-interference ratio analysis," Journal of Communications and Networks, vol. 20, no. 5, pp. 484–495, 2018.

[15] K. Yoshikawa, K. Yamamoto, T. Nishio, and M. Morikura, "Grid-based exclusive region design for 3D UAV networks: A stochastic geometry approach," IEEE Access, vol. 7, pp. 103 806–103 814, 2019.

[16] H. Wu, X. Tao, N. Zhang, and X. Shen, "Cooperative UAV cluster-assisted terrestrial cellular networks for ubiquitous coverage," IEEE Journal on Selected Areas in Communications, vol. 36, no. 9, pp. 2045–2058, 2018.

[17] C. Saha, M. Afshang, and H. S. Dhillon, "Enriched k-tier HetNet model to enable the analysis of user-centric small cell deployments," IEEE Transactions on Wireless Communications, vol. 16, no. 3, pp. 1593–1608, 2017.

[18] M. Afshang and H. S. Dhillon, "Poisson cluster process based analysis of HetNets with correlated user and base station locations," IEEE Transactions on Wireless Communications, 2018.

[19] C. Saha, M. Afshang, and H. S. Dhillon, "Poisson cluster process: Bridging the gap between PPP and 3GPP HetNet models," in Information Theory and Applications Workshop (ITA), 2017. IEEE, 2017, pp. 1–9.

[20] W. Yi, Y. Liu, Y. Deng, and A. Nallanathan, "Clustered UAV networks with millimeter Wave communications: A stochastic geometry view," IEEE Transactions on Communications, 2020.

[21] W. Yi, Y. Liu, A. Nallanathan, and G. K. Karagiannidis, "A unified spatial framework for clustered UAV networks based on stochastic geometry," in Proc. of IEEE Global Communications Conference (GLOBECOM), 2018, pp. 1–6.

[22] A. M. Hayajneh, S. A. R. Zaidi, D. C. McLernon, M. Di Renzo, and M. Ghogho, "Performance analysis of UAV enabled disaster recovery

networks: A stochastic geometric framework based on cluster processes," IEEE Access, vol. 6, pp. 26 215–26 230, 2018.
[23] N. Cherif, M. Alzenad, H. Yanikomeroglu, and A. Yongacoglu, "Downlink coverage and rate analysis of an aerial user in integrated aerial and terrestrial networks," arXiv preprint arXiv:1905.11934, 2019.
[24] Y. Sun, T. Wang, and S. Wang, "Location optimization and user association for unmanned aerial vehicles assisted mobile networks," IEEE Transactions on Vehicular Technology, vol. 68, no. 10, pp. 10 056–10 065, 2019.
[25] R. K. Ganti and M. Haenggi, "Interference and outage in clustered wireless Ad Hoc networks," IEEE Transactions on Information Theory, vol. 55, no. 9, pp. 4067–4086, 2009.
[26] A. Omri, M. O. Hasna, M. Z. Shakir, and M. Shaqfeh, "3-D placement schemes of multiple UAVs in NFP-based wireless networks," in 2018 5th International Conference on Information and Communication Technologies for Disaster Management (ICT-DM). IEEE, 2018, pp. 1–5.
[27] K. Smiljkovikj, H. Elshaer, P. Popovski, F. Boccardi, M. Dohler, L. Gavrilovska, and R. Irmer, "Capacity analysis of decoupled downlink and uplink access in 5G heterogeneous systems," arXiv preprint arXiv:1410.7270, 2014.
[28] K. Smiljkovikj, P. Popovski, and L. Gavrilovska, "Analysis of the decoupled access for downlink and uplink in wireless heterogeneous networks," IEEE Wireless Communications Letters, vol. 4, no. 2, pp. 173–176, 2015.
[29] N. Sial and J. Ahmed, "A novel and realistic hybrid downlink-uplink coupled/decoupled access scheme for 5G HetNets," Turkish Journal of Electrical Engineering & Computer Sciences, vol. 25, no. 6, pp. 4457–4473, 2017.
[30] M. Bacha, Y. Wu, and B. Clerckx, "Downlink and uplink decoupling in two-tier heterogeneous networks with multi-antenna base stations," IEEE Transactions on Wireless Communications, vol. 16, no. 5, pp. 2760–2775, 2017.
[31] K. Smiljkovikj, L. Gavrilovska, and P. Popovski, "Efficiency analysis of downlink and uplink decoupling in heterogeneous networks," in Proc. of IEEE Communication Workshop (ICCW), 2015, pp. 125–130.
[32] L. Zhang, W. Nie, G. Feng, F.-C. Zheng, and S. Qin, "Uplink performance improvement by decoupling uplink/downlink access in HetNets," IEEE Transactions on Vehicular Technology, vol. 66, no. 8, pp. 6862–6876, 2017.
[33] M. Arif, S. Wyne, and J. Ahmed, "Performance analysis of downlink and uplink decoupled access in clustered heterogeneous cellular networks," Telecommunication Systems, vol. 72, pp. 355–364, 2019.
[34] Z. Sattar, J. V. Evangelista, G. Kaddoum, and N. Batani, "Spectral efficiency analysis of the decoupled access for downlink and uplink in two-tier network," IEEE Transactions on Vehicular Technology, vol. 68, no. 5, pp. 4871–4883, 2019.
[35] K. P. Peppas, F. Lazarakis, A. Alexandridis, and K. Dangakis, "Simple, accurate formula for the average bit error probability of multiple-input multiple-output free-space optical links over negative exponential turbulence channels," Optics letters, vol. 37, no. 15, pp. 3243–3245, 2012.
[36] K. P. Peppas, "A new formula for the average bit error probability of dual-hop amplify-and-forward relaying systems over generalized shadowed fading channels," IEEE Wireless Communications Letters, vol. 1, no. 2, pp. 85–88, 2012.
[37] E. Turgut and M. C. Gursoy, "Downlink analysis in unmanned aerial vehicle (UAV) assisted cellular networks with clustered users," IEEE Access, vol. 6, pp. 36 313–36 324, 2018.
[38] S. N. Chiu, D. Stoyan, W. S. Kendall, and J. Mecke, Stochastic geometry and its applications. John Wiley & Sons, 2013.
[39] A. A. Kilbas, H-transforms: Theory and Applications. CRC Press, 2004.
[40] Y. Wang and Q. Zhu, "Modeling and analysis of small cells based on clustered stochastic geometry," IEEE Communications Letters, vol. 21, no. 3, pp. 576–579, 2017.
[41] K. Katsalis, N. Nikaein, E. Schiller, A. Ksentini, and T. Braun, "Network slices toward 5G communications: Slicing the LTE network," IEEE Communications Magazine, vol. 55, no. 8, pp. 146–154, 2017.
[42] Y.-i. Choi and N. Park, "Slice architecture for 5G core network," in 2017 Ninth international conference on ubiquitous and future networks (ICUFN). IEEE, 2017, pp. 571–575.
[43] H. Wei, Z. Zhang, and B. Fan, "Network slice access selection scheme in 5G," in 2017 IEEE 2nd Information Technology, Networking, Electronic and Automation Control Conference (ITNEC). IEEE, 2017, pp. 352–356.
[44] G. Brown, "Service-based architecture for 5G core networks," A Heavy Reading white paper produced for Huawei Technologies Co. Ltd. Online verfugbar unter: https://www. huawei. com/en/press-events/news/2017/11/HeavyReading-WhitePaper-5G-Core-Network, letzter Zugriff am, vol. 1, p. 2018, 2017.
[45] A. Lucent, "Introduction to evolved packet core," white paper, vol. 12, 2009.
[46] T.-X. Do and Y. Kim, "Control and data plane separation architecture for supporting multicast listeners over distributed mobility management," ICT Express, vol. 3, no. 2, pp. 90–95, 2017.
[47] B. A. A. Nunes, M. Mendonca, X.-N. Nguyen, K. Obraczka, and T. Turletti, "A survey of software-defined networking: Past, present, and future of programmable networks," IEEE Communications Surveys & Tutorials, vol. 16, no. 3, pp. 1617–1634, 2014.
[48] J. G. Andrews, F. Baccelli, and R. K. Ganti, "A tractable approach to coverage and rate in cellular networks," IEEE Transactions on communications, vol. 59, no. 11, pp. 3122–3134, 2011.
[49] P. Mittal and K. Gupta, "An integral involving generalized function of two variables," in Proceedings of the Indian academy of sciences-section A, vol. 75, no. 3. Springer, 1972, pp. 117–123.

MOHAMMAD ARIF received his B.S. degree from University of Engineering and Technology, Peshawar, Pakistan in 2012 and the M.S. degree from the COMSATS University Islamabad (CUI), Islamabad, Pakistan, in 2014. Currently, he is pursuing the Ph.D. degree from the Department of Electrical and Computer Engineering, CUI, Islamabad, Pakistan.

His research interests include aerial and terrestrial heterogeneous cellular networks, dual connectivity, uplink and downlink interference management, indoor localization, signal processing, and channel coding.

SHURJEEL WYNE (S'02−M'08−SM'13) received his Ph.D. degree from Lund University, Sweden, in 2009. From 2009 to 2010, he was a Postdoctoral Research Fellow, funded by the High-Speed Wireless Center, Lund University. Since 2010, he is with the Department of Electrical and Computer Engineering, COMSATS University Islamabad (CUI), Islamabad, Pakistan, where he is currently an Associate Professor.

His research interests include wireless channel characterization, multi-antenna systems, cooperative communications, physical layer security, and vehicular communications. He was a co-recipient of the Best Paper Award of the Antennas and Propagation Track at the IEEE VTC2013-Spring.

KEIVAN NAVAIE is currently with the School of Computing and Communications, Lancaster University, U.K. His research interests include provisioning dependable connectivity and positioning to intelligent cyber-physical systems. He is a Fellow of the IET, a Senior Fellow of the HEA, and a Chartered Engineer in the U.K. He currently serves on the Editorial Board of the IEEE TRANSACTIONS ON WIRELESS COMMUNICATIONS, the IEEE COMMUNICATIONS LETTERS, and the IEEE COMMUNICATIONS SURVEYS AND TUTORIAL.

SYED JUNAID NAWAZ (S'08–M'12–SM'16) received the Ph.D. degree in electronic engineering from Mohammad Ali Jinnah University, Islamabad, in February 2012. Since September 2005, he has worked on several research and teaching positions with COMSATS University Islamabad (CUI), Pakistan; Staffordshire University, UK; Federal Urdu University, Pakistan; The University of York, UK; and Aristotle University of Thessaloniki, Greece. He is currently working as an Assistant Professor with the Department of Electrical and Computer Engineering, COMSATS University Islamabad (CUI), Islamabad, Pakistan.

His current research interests include physical channel modeling, channel estimation and characterization, mMIMO systems, adaptive signal processing, machine learning, compressed sensing, mmWave channels, airborne internet, internet of things, and vehicle-to-vehicle communications.

SAJID HUSSAIN ALVI received his MSc and MPhil degrees in Electronics from Quaid-e-Azam University Islamabad, Pakistan in 2001 and 2006, respectively. He received his PhD from Department of Electrical Engineering, COMSATS Institute of Information Technology (CIIT), presently COMSATS University Islamabad (CUI), Islamabad, Pakistan in 2017. From 2004-2006, he served as a lecturer at the Department of Electrical Engineering, AIR University Islamabad, Pakistan. Since 2006 he is serving as a faculty member at CUI where he is currently an assistant professor at the Department of Physics. Dr. Alvi's research interests are in cooperative communications, terrestrial and aerial heterogeneous networks, and signal processing.